

# Topographic mapping of VMH → arcuate nucleus microcircuits and their reorganization by fasting

Scott M Sternson<sup>1</sup>, Gordon M G Shepherd<sup>2</sup> & Jeffrey M Friedman<sup>1</sup>

In the hypothalamic arcuate nucleus (ARC), pro-opiomelanocortin (POMC) neurons inhibit feeding and neuropeptide-Y (NPY) neurons stimulate feeding. We tested whether neurons in the ventromedial hypothalamic nucleus (VMH), a known satiety center, activate anorexigenic neuronal pathways in the ARC by projecting either excitatory synaptic inputs to POMC neurons and/or inhibitory inputs to NPY neurons. Using laser scanning photostimulation in brain slices from transgenic mice, we found that POMC and NPY neurons, which are interspersed in the ARC, are nevertheless regulated by anatomically distinct synaptic inputs. POMC neurons received strong excitatory input from the medial VMH (mVMH), whereas NPY neurons did not and, instead, received weak inhibitory input only from within the ARC. The strength of the excitatory input from the mVMH to POMC neurons was diminished by fasting. These data identify a new molecularly defined circuit that is dynamically regulated by nutritional state in a manner consistent with the known role of the VMH as a satiety center.

The hypothalamus regulates food intake and body weight<sup>1</sup>. Classic brain lesioning experiments led to a ‘two-center’ hypothesis in which the ventromedial hypothalamic nucleus (VMH) signals satiety<sup>2</sup> and the lateral hypothalamus signals hunger<sup>3</sup> (Fig. 1a). Although the lesions in these studies also affected surrounding brain regions, precise genetic disruption of the VMH by a mutation in the gene encoding steroidogenic factor-1 has confirmed the importance of the VMH in maintaining energy homeostasis<sup>4</sup>. Recently, numerous molecular and genetic experiments have also identified the hypothalamic arcuate nucleus (ARC) as a critical regulator of energy balance<sup>5</sup>. Within the ARC, discrete populations of NPY and POMC neurons sense hormonal and metabolic signals and activate homeostatic responses that favor energy storage or energy dissipation<sup>6–9</sup>. In addition to sensing peripheral metabolic signals, these key, molecularly defined regulatory neurons receive synaptic inputs from other brain regions<sup>10,11</sup>. However, the sources of many of these inputs have not been determined. Based on data from lesioning studies, we reasoned that some of these inputs might come from the VMH.

Although the VMH was first identified as a satiety center more than 60 years ago, the mechanism by which it regulates satiety and body weight is largely unknown<sup>2</sup>. In these studies, we considered the possibility that the VMH regulates energy balance by modulating the activity of discrete populations of neurons in the ARC. Specifically, we set out to delineate the functional connections between the VMH and the ARC with the aim of integrating the classic neuroanatomic studies of Hetherington and Ranson<sup>2</sup> with the more recent identification of molecularly defined neuronal populations in the ARC. The VMH is adjacent to the ARC (Fig. 1a), but synaptic inputs from the VMH to

POMC or NPY neurons in the ARC have not been reported. Although injection of an anterograde neuronal tracer into the VMH does not label the ARC, the cell-poor region separating the VMH and the dorsal surface of the ARC does reveal heavy innervation<sup>12</sup> (see Figs. 3 L-O and 4G-I in ref. 12). Other studies show that Golgi-stained ARC neurons project dendrites as a ‘shell’ along this dorsal ARC surface<sup>13</sup>, suggesting that there are potential sites of interaction between the VMH and ARC. We thus considered the hypothesis that VMH neurons activate anorexigenic neuronal pathways in the ARC by projecting excitatory synaptic inputs to POMC neurons and/or inhibitory inputs to NPY neurons.

To identify the microcircuits within hypothalamic feeding centers, we used laser scanning photostimulation<sup>14–21</sup> (LSPS) to map the distributions of presynaptic partners in the VMH onto individual neurons in the ARC (Fig. 1b). LSPS measures the origin and strength of functional synaptic projections to individual neurons within a brain slice by stimulating small clusters of presynaptic neurons with glutamate uncaging while simultaneously recording evoked postsynaptic currents (PSCs) in whole-cell voltage clamp. The reversal potential of the evoked current is used to characterize the connection as excitatory or inhibitory. Uncaging glutamate can give rise to three types of responses in the recorded neuron (Fig. 1c). First, a direct response occurs when glutamate uncaging occurs near the soma or dendrites of the voltage-clamped neuron, directly activating glutamate receptors. Second, a synaptic response (that is, a PSC) occurs when glutamate uncaging activates a presynaptic neuron to fire an action potential, which induces neurotransmitter release, resulting in an evoked synaptic current in the voltage-clamped neuron (Fig. 1d). Third, no response is observed at sites of glutamate uncaging that do not

<sup>1</sup>Howard Hughes Medical Institute and Laboratory of Molecular Genetics, The Rockefeller University, 1230 York Ave., New York, New York 10021, USA. <sup>2</sup>Howard Hughes Medical Institute and Cold Spring Harbor Laboratory, Cold Spring Harbor, New York 11724. Correspondence should be addressed to J.M.F. (friedj@rockefeller.edu).

Received 21 July; accepted 25 August; published online 18 September 2005; doi:10.1038/nn1550

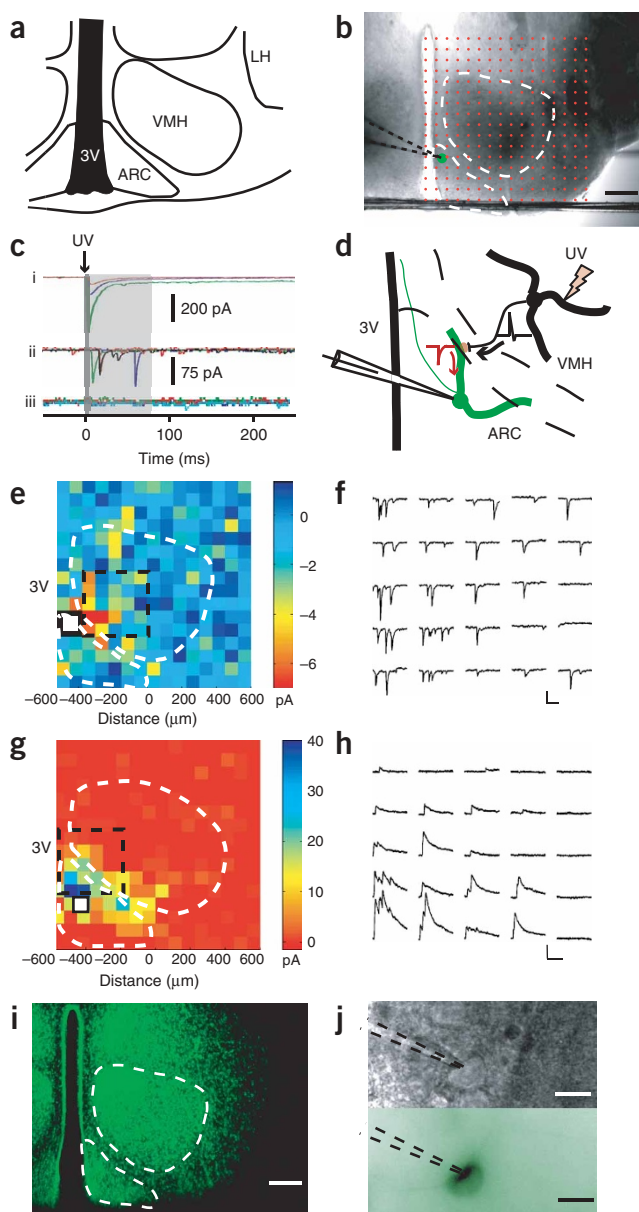


**Figure 1** Laser scanning photostimulation for mapping hypothalamic neural circuits. **(a)** Hypothalamic brain regions that were studied. 3V: third ventricle. **(b)** Brain slice of mediobasal hypothalamus (300  $\mu\text{m}$  thick). The boundaries of the ARC and VMH are indicated. Red circles: laser stimulation sites. Green circle: voltage-clamped soma. The patch pipette is marked with a dashed black outline. Scale bar equals 300  $\mu\text{m}$ . **(c)** Three types of responses observed in LSPS. (i) Direct response. Dark gray bar marks 0–5 ms. (ii) Synaptic response. Light gray shading marks 5–75 ms. (iii) No response. **(d)** Focal glutamate release near the soma or dendrite causes action potential firing and neurotransmitter release (pink ball) which is detected as a postsynaptic current (red). **(e)** Map of synaptic responses to photostimulation. Colors represent mean synaptic current measured 5–75 ms after photostimulation. Black pixels: direct responses. White square: soma position. Dotted white lines define anatomical boundaries from individual brain slices. **(f)** Examples of individual postsynaptic currents from black boxed region of **e**. Scale bars: 35 pA, 25 ms. **(g)** From a different neuron, inhibitory synaptic input map. **(h)** Examples of individual inhibitory postsynaptic currents resulting from glutamate uncaging from black boxed region of **g**. Scale bars: 35 pA, 125 ms. **(i)** Fluorescence micrograph (false-color image) of a fixed brain slice stained with Sytox Green was used to define nuclear boundaries, post-recording. Scale bar: 300  $\mu\text{m}$ . **(j)** Voltage-clamped neuron under infrared gradient contrast optics (top) and during fluorescence emission (bottom, false-color image), identifying it as a POMC cell. Scale bars: 15  $\mu\text{m}$ .

allowing a 1.3 mm<sup>2</sup> region of the neuropil to be rapidly assayed for sites of connectivity (**Fig. 1b**). For each stimulation site, the strength of the connection was calculated as the average current response (in pA) following stimulation. The connection strengths at each stimulation site were used to generate a map of the monosynaptic connections to individual POMC or NPY neurons, where each site corresponds to a pixel position in the map (**Fig. 1e–h**). Anatomical boundaries were determined post-recording (**Fig. 1i**) and overlaid onto synaptic input maps. We distinguished POMC and NPY neuronal subtypes using mice with a bacterial artificial chromosome transgene containing either *pomc* or *npy* genomic sequence (plus ~200 kb flanking sequence) modified to express green fluorescent protein (GFP) so that the cell type was labeled and could be identified by fluorescence emission<sup>10</sup> (**Fig. 1j**). Thus, by combining LSPS with cell type-specific GFP expression, we could determine if neuronal microcircuits were specifically associated with molecularly defined neuronal cell types. Such distinct circuits might be predicted based on the opposing functions of POMC and NPY neurons. To represent the observed projections to POMC, NPY and unlabeled cells, we denote cell type (when known), anatomic location, and the sign of functional connectivity. For example,  $\text{mVMH}^{\text{exc}} \rightarrow \text{ARC}^{\text{POMC}}$  describes a connection in which the mVMH projects excitatory synapses to POMC neurons in the ARC (see below).

### Resolution of photostimulation mapping in the hypothalamus

LSPS is used to identify presynaptic neuron location by glutamate stimulation of action potentials in presynaptic neurons that results in a postsynaptic current response in the voltage-clamped neuron (**Fig. 1f**). The spatial distribution of uncaging sites that produce action potentials in a presynaptic neuron defines the effective resolution for mapping the origin of the synaptic responses. Because somatic and dendritic glutamate stimulation can generate action potentials, the resolution with which presynaptic neuron location can be determined depends, in part, on both neuronal structure and membrane properties. Thus, control experiments are required to determine if there are differences in the responsiveness to glutamate uncaging in the areas that will be investigated for synaptic mapping.

To determine the spatial distribution of uncaging sites around a neuron that elicited action potentials, we constructed excitation

contain neurons connected to the voltage-clamped neuron. Note that under the conditions used here, only monosynaptic inputs were observed (see below).

Overall, LSPS provides an unbiased means for locating presynaptic neurons and has been well validated as a method for discovery of new circuit connections<sup>15,17</sup>. For this purpose, LSPS has advantages relative to other approaches such as electrical stimulation, which is limited by uncertainty about the origin of connections because axons of passage are also stimulated, and paired recordings, which are inefficient due to low connection probabilities and the corresponding paucity of connections that can be sampled per experiment. Previously, LSPS has been used to map cortical<sup>15–17,20</sup> and hippocampal<sup>18</sup> circuits, but it has not yet been applied to mapping hypothalamic circuits.

## RESULTS

In this study, glutamate uncaging was repeated at 256 discrete points across a brain slice (300  $\mu\text{m}$  thick) that included the ARC and VMH,

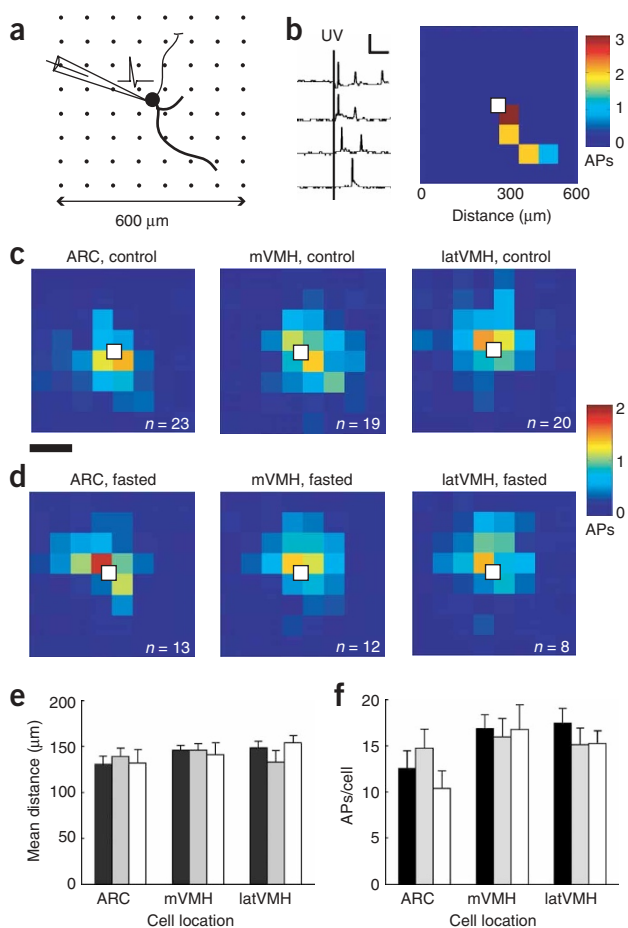


**Figure 2** Excitation profiles and resolution of stimulation by glutamate uncaging. **(a)** Loose-seal extracellular recording of action potentials after uncaging glutamate in a grid pattern around somata neuron defines the spatial extent over which action potentials can be generated. **(b)** Action potentials (APs) resulting from glutamate uncaging. The uncaging sites that evoked action potentials are mapped and color-coded for the number of action potentials. Scale bars equal 1 mV, 25 ms. **(c,d)** Average excitation profiles for neurons in the ARC, mVMH and latVMH under **(c)** control conditions and **(d)** in fasted mice. Scale bar: 150 μm. **(e)** Average resolution of photostimulation. Resolution was determined by calculating the weighted mean distance ( $R$ ) to an action potential ( $R = \Sigma(r \times n) / \Sigma n$ , where  $r$  is the distance to the soma for each stimulation site and  $n$  is the number of action potentials at that site) in excitation profiles from neurons in the ARC, mVMH and latVMH. **(f)** Average excitability to glutamate uncaging. The glutamate excitability of neurons in each region was calculated from excitation profiles as the total number of action potentials measured for each cell (APs/cell). Black bars: control conditions, gray bars: fasted conditions, white bars: *ob/ob*. Error bars are s.e.m.

Also, for synaptic maps, the magnitude of the response in the voltage-clamped neuron is dependent, in part, on the number of action potentials generated in the presynaptic neuron in response to glutamate uncaging (glutamate excitability)<sup>17</sup>. The glutamate excitability was ~12–16 action potentials/cell for the ARC, mVMH and latVMH (Fig. 2f), and the differences were not statistically significant. Thus, in synaptic mapping, differences in the strength of inputs from these anatomically separate regions (see below) were not attributable to differences in either glutamate excitability or the resolution of glutamate uncaging.

We also established that LSPS, under the conditions used here, measures only monosynaptic connections between an uncaging site and the voltage-clamped neuron (as opposed to activating a polysynaptic chain of neurons). Excitation profiles with and without calcium in the bath were used to confirm that synaptic input resulting from focal uncaging of glutamate was not sufficient to evoke action potentials. Comparison of excitation profiles recorded in ~0 mM  $\text{Ca}^{2+}$ /8 mM  $\text{Mg}^{2+}$  with those for the same cell in 4 mM  $\text{Ca}^{2+}$ /4 mM  $\text{Mg}^{2+}$  did not show any additional sites of evoked action potentials in neurons recorded from the ARC, mVMH and latVMH (data not shown). Under low  $\text{Ca}^{2+}$ , a condition under which synaptic transmission is improbable, the excitation profile could only represent direct stimulation of the recorded neuron with no contribution from synaptic input. We did not observe any additional sites of action potential generation when synaptic transmission was enabled by calcium, indicating that synaptic input maps represent only monosynaptic connections.

These control experiments demonstrated that LSPS is well-suited for mapping distributions of monosynaptic inputs to hypothalamic neurons and that the mapping resolution was sufficient to permit presynaptic neuron location to be determined within subregions of hypothalamic nuclei. Thus, using LSPS, we set out to identify functional connections from the VMH to ARC neurons involved in regulating energy homeostasis.

### Excitatory synaptic input maps

We first surveyed the overall excitatory VMH inputs to the ARC by recording from a set of unlabeled ARC neurons ( $n = 16$ ) in which neuronal subtype was not identified. Unlabeled ARC neurons included POMC, NPY and other ARC neuronal subtypes. The stimulation sites were recorded in the same orientation for different cells, allowing maps of multiple cells to be averaged (example maps for individual cells in this group are shown in Fig. 3, top). The resulting group input map showed the regions that gave rise to the strongest and most consistent

profiles<sup>17</sup> by recording evoked action potentials (loose-seal extracellular recordings) after stimulation by focal uncaging of glutamate in a grid pattern of stimulation sites centered on the soma (Fig. 2a). The spatial location and the number of evoked action potentials were represented in a color map (Fig. 2b). Excitation profiles were generated for multiple neurons in three brain regions: ARC, medial VMH (mVMH) and lateral VMH (latVMH). Average excitation profiles (Fig. 2c,d) portrayed the spatial distribution of glutamate responsiveness (the resolution of photostimulation) in each of these areas. These excitation profiles demonstrated that the strongest activation is at sites adjacent to the soma, with a fall-off in responsiveness at more distant secondary sites. We quantified the resolution as the weighted mean distance ( $R$ ) from the soma to each site of action potential stimulation ( $R = \Sigma(r \times n) / \Sigma n$ , where  $r$  is the distance to the soma for each stimulation site and  $n$  is the number of action potentials at that site). The mean resolution was ~140 μm for the ARC, mVMH and latVMH under fed and fasted conditions and for *ob/ob* mice (Fig. 2e). Thus, in synaptic maps, a connected presynaptic neuron may be expected to generate a post-synaptic response not only at the location of its soma but also, on average, within two stimulation sites surrounding the soma, as seen in excitation profiles. This resolution is less refined than that reported in barrel cortex neurons (~50% greater than for layer 4 and layer 5 neurons in ref. 17). This may be related to the very high membrane resistance in these hypothalamic neurons (typically >1 GΩ), which might be expected to enhance the excitability of these neurons from stimulation at more distal dendritic sites if this results in a larger membrane length constant and increased electrotonic conduction.

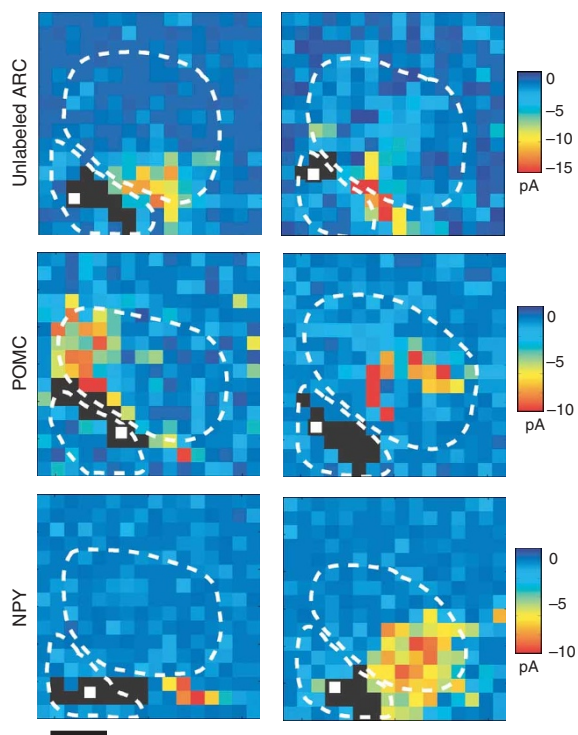


**Figure 3** Synaptic input maps for individual unlabeled ARC, POMC and NPY neurons. Maps were repeated two to four times and averaged for each neuron. Dotted white lines define anatomical boundaries from individual brain slices. Black pixels: direct responses. White square: soma position. Scale bar: 300  $\mu\text{m}$ .

excitatory presynaptic inputs to these ARC neurons. For unlabeled ARC neurons, the excitatory synaptic input (**Fig. 4a**, left) was broadly distributed across both the VMH and the ARC with the strongest concentration of inputs coming from the latVMH (**Fig. 4a**, left, arrowhead). There were also excitatory inputs originating within the ARC as well as the mVMH, and inspection of input maps to individual cells showed that a small subset of unlabeled neurons received input predominantly from the mVMH (4/16). However, these were diluted in the average synaptic map for the entire sample of unlabeled ARC neurons by the input distributions of the other cells. We refer to these VMH projections as  $\text{VMH}^{\text{exc}} \rightarrow \text{ARC}^{\text{unknown}}$ , denoting the lack of knowledge about the identity of the postsynaptic cell. These results are the first demonstration of direct, functional inputs from the VMH to the ARC, highlighting the usefulness of LSPS for identifying new circuit elements. This sample of input distributions onto unlabeled ARC neurons also provided a basis for comparisons to the input distributions generated by recordings from molecularly defined neurons.

We next focused on inputs to the POMC neurons in slices from *pomc-gfp* BAC transgenic mice (**Fig. 4a**, middle). The origin of excitatory projections to POMC neurons ( $n = 24$ ) was concentrated as a 'hotspot', primarily within the mVMH (boxed in **Fig. 4a**, mean synaptic input from boxed region:  $-4.2 \pm 0.9$  pA/stimulation site), with additional, sparse inputs from elsewhere in the mVMH, ARC and periventricular regions. A few neurons also received input from the latVMH (**Fig. 3**, middle). Projections from the mVMH represented a subset of the input distribution evident when recording from unlabeled neurons in the ARC, and the  $\text{mVMH}^{\text{exc}} \rightarrow \text{ARC}^{\text{POMC}}$  projection was significantly stronger than projections from the corresponding region in

$\text{mVMH}^{\text{exc}} \rightarrow \text{ARC}^{\text{unknown}}$  (**Fig. 4c**,  $P < 0.03$ , Mann-Whitney). This observation suggests that in the studies of unlabeled neurons, the strength of the  $\text{mVMH}^{\text{exc}} \rightarrow \text{ARC}^{\text{POMC}}$  projection was diluted by projections originating elsewhere and targeting other cell types that were represented in the sample of unlabeled ARC neurons. Overall, these data show that the mVMH contains a group of neurons that preferentially form excitatory synapses onto POMC neurons relative to other ARC neurons. This result also shows that recording from molecularly defined, labeled cell types can demonstrate specific spatial patterns of presynaptic input that are not evident when recording from unlabeled neurons.

The pattern of inputs to the arcuate NPY neurons was markedly different from both the inputs to the POMC and unlabeled neurons. The average excitatory input to NPY neurons ( $n = 16$ ) was significantly less than for POMC or unlabeled ARC neurons ( $P < 0.02$ , Dunn's Test). The spatial distribution was different than for POMC neurons, with the inputs originating from within the ARC and the latVMH (**Fig. 4a**, right, arrow). Many NPY neurons did not receive evoked synaptic input, but a subset of the neurons (5/16) did show excitatory inputs originating from the latVMH and adjacent lateral regions (**Fig. 3**, bottom). Notably, mVMH excitatory synaptic input to NPY neurons was absent, indicating that the  $\text{mVMH}^{\text{exc}} \rightarrow \text{ARC}^{\text{POMC}}$  and  $\text{latVMH}^{\text{exc}} \rightarrow \text{ARC}^{\text{NPY}}$  circuits are distinct. Note, however, that medial inputs to NPY neurons were observed in some slices from a more caudal region containing the dorsomedial hypothalamic nucleus directly adjacent to the ARC (S.M.S. and J.M.F., unpublished data). Thus, although POMC and NPY neurons are interspersed in the ARC, they nevertheless receive anatomically distinct synaptic inputs.

### Inhibitory synaptic input maps

We also mapped inhibitory synaptic inputs (**Figs. 1i,j** and **4b**). POMC and unlabeled ARC neurons received the same total amount of inhibitory synaptic input with similar spatial distributions (**Fig. 4d**, mean synaptic input from the ARC: POMC,  $3.0 \pm 0.7$  pA/stimulation site; unlabeled ARC,  $3.6 \pm 0.7$  pA/stimulation site). Inhibitory inputs arose primarily from the ARC with only weak average inhibitory input strength from within the VMH. On the basis of ultrastructure analysis, POMC neurons receive inhibitory, GABA-containing synapses from NPY neurons<sup>22</sup>, and the pattern of local ARC inhibition found here is consistent with this. However, it is likely that other inhibitory cell types are also involved. For example, we observed that the ventromedial ARC, which has a high density of NPY neurons, was not a substantial source of synaptic inhibition to the POMC and unlabeled neurons (**Fig. 4b**). The identity of the non-NPY cells projecting inhibitory inputs onto the POMC neurons is not known.

We found only weak inhibitory synaptic projections to NPY neurons (**Fig. 4b**, right), and these originated almost exclusively from within the ARC (**Fig. 4d**, mean synaptic input from the ARC:  $1.0 \pm 0.3$  pA/stimulation site,  $P < 0.02$ , Dunn's Test). This weak synaptic input to NPY neurons is consistent with a study that showed significantly lower synapse density on NPY neurons relative to POMC neurons<sup>10</sup>. Notably, inhibitory synaptic input onto NPY neurons was not observed coming from the VMH. This observation mitigates the possibility that the VMH reduces food intake by directly projecting inhibitory synapses to NPY neurons and suggests that the VMH is more likely to contribute to satiety by activating POMC neurons via  $\text{mVMH}^{\text{exc}} \rightarrow \text{ARC}^{\text{POMC}}$  rather than by inhibiting orexigenic NPY neurons.

### Fasting markedly reduces $\text{mVMH}^{\text{exc}} \rightarrow \text{ARC}^{\text{POMC}}$

The presence of an excitatory circuit projection between the mVMH and POMC neurons ( $\text{mVMH}^{\text{exc}} \rightarrow \text{ARC}^{\text{POMC}}$ ) suggests a possible role for this circuit in mediating the ability of the VMH to reduce food

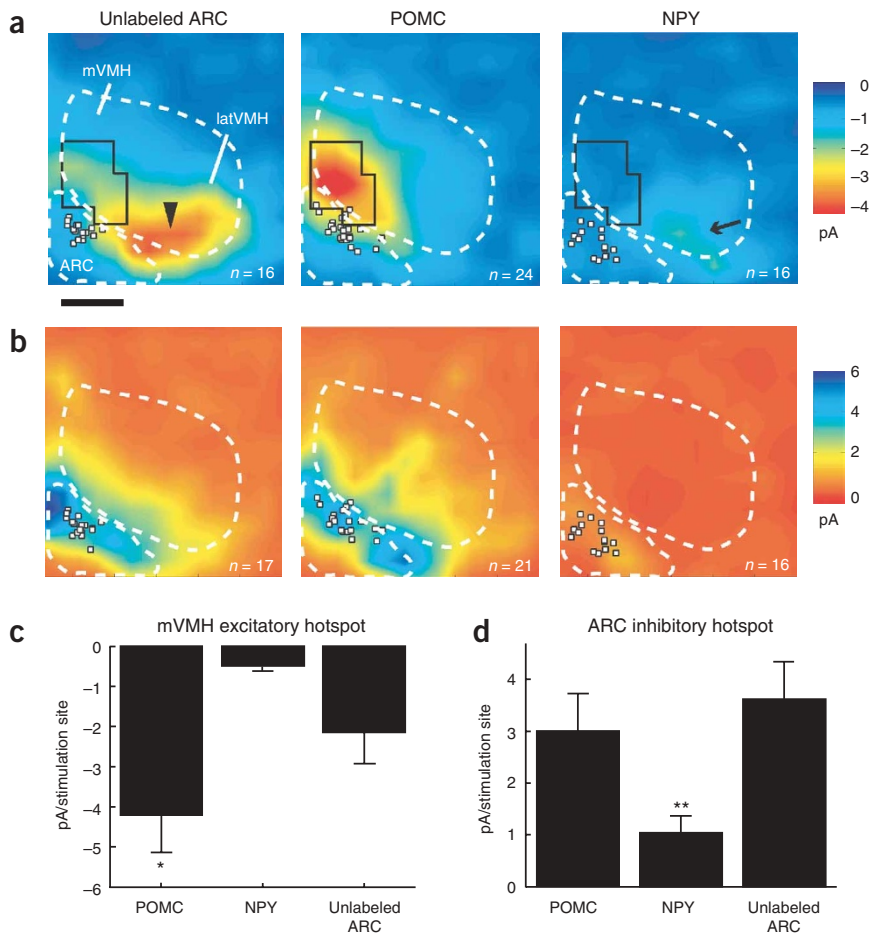


**Figure 4** Mean synaptic input maps for unlabeled ARC, POMC and NPY neurons show the strengths and distinct spatial distributions of synaptic inputs onto these neuronal populations. **(a)** Excitatory input maps. The black box defines the boundaries of the mVMH hotspot. Arrowhead marks the location of the concentration of inputs to unlabeled ARC neurons; arrow denotes a concentration of inputs to NPY neurons. White squares mark soma location. Scale bar: 300  $\mu$ m. **(b)** Inhibitory input maps. **(c,d)** Mean synaptic input to unlabeled ARC, POMC and NPY neurons from **(c)** the mVMH excitatory hotspot and **(d)** from the ARC inhibitory hotspot, which is defined by the anatomical boundary of the ARC. \*,  $P < 0.03$ , Mann-Whitney comparison with unlabeled ARC. \*\*,  $P < 0.02$ , Dunn's Test). Error bars are s.e.m.

center and suggests that this projection may have a functional role to increase feeding after food restriction.

#### Leptin does not block reduction of $mVMH^{exc} \rightarrow ARC^{POMC}$

The response to fasting includes changes in the levels of a number of hormonal and metabolic signals including leptin, which decreases significantly with fasting<sup>23</sup>. To test whether the altered inputs to the POMC neurons resulted from the decreased leptin concentration associated with food deprivation and weight loss, we treated fasted animals with leptin as previously described<sup>23</sup>. In this case, average excitatory synaptic input strength of  $mVMH^{exc} \rightarrow ARC^{POMC}$  (Fig. 5c) was similar to that from the fasted animals that did not receive leptin

intake. To correlate the strength of the  $mVMH^{exc} \rightarrow ARC^{POMC}$  projection with changes in nutritional state, we mapped the synaptic inputs to POMC neurons after food deprivation. If synaptic circuits have a role in regulating feeding, the connection strength might be expected to decrease in  $mVMH^{exc} \rightarrow ARC^{POMC}$  and/or increase in  $ARC^{inh} \rightarrow ARC^{POMC}$ . Mice were fasted for 24 h, over which time they lost  $17 \pm 0.8\%$  of their body weight. In fasted animals, there was a significant reduction in the strength of  $mVMH^{exc} \rightarrow ARC^{POMC}$  relative to the strength of that projection in fed mice (mean synaptic input from boxed region:  $-2.1 \pm 0.6$  pA/stimulation site,  $P = 0.03$ , Mann-Whitney; Fig. 5a). Control experiments ruled out differences in the intrinsic responsiveness of mVMH neurons to glutamate stimulation after fasting as a cause of this reduction (Fig. 2c–f). To visualize sites of circuit plasticity, we computed difference maps by subtracting the average excitatory synaptic input map for POMC neurons in fasted mice from that of fed mice. This showed a significant difference in the strength of the  $mVMH^{exc} \rightarrow ARC^{POMC}$  circuit between these two states (Fig. 5d). In addition, a small but significant gain of spatially distinct excitatory synaptic inputs to POMC neurons arising from the lateral ARC/VMH boundary was observed (Fig. 5d,f, region of interest 4). The total inhibitory synaptic inputs to POMC neurons from the ARC,  $ARC^{inh} \rightarrow ARC^{POMC}$ , were not significantly different in fasted mice relative to the fed state (Fig. 5g,i). These data show that the mVMH excitatory connections to POMC neurons show marked plasticity with food deprivation (Fig. 5f, regions of interest 1–3). The demonstration that the  $mVMH^{exc} \rightarrow ARC^{POMC}$  projection is downregulated by fasting is also consistent with the known role of the VMH as a satiety

(mean synaptic input from mVMH hotspot:  $-1.3 \pm 0.2$  pA/stimulation site,  $P > 0.7$ , Mann-Whitney; also Fig. 5f, regions of interest 1–3). These data suggest that low leptin levels are unlikely to be directly responsible for the change associated with fasting in synaptic connections between mVMH neurons and POMC neurons associated with fasting and that some other signal is responsible. Consistent with this, group excitatory synaptic input maps from leptin-deficient *ob/ob*, *pomc-gfp* mice (Fig. 5c,f) were not different from those from fed, wild-type *pomc-gfp* mice, further indicating that this projection is also not affected by leptin deficiency. Inhibitory inputs to POMC neurons were also unchanged with leptin treatment of fasted mice (Fig. 5h,i). However, the site of increased excitatory input to POMC neurons from the latARC/VMH was no longer evident when fasted animals received leptin (Fig. 5d–f, region of interest 4). Thus, this small hotspot, which is identified only after fasting, seems to be leptin regulated. The functional role of this projection is unclear, as it is not seen in other POMC synaptic input maps, and on the basis of the sign of this connection, it would be expected to paradoxically reduce food intake in fasted animals. Alternatively, this projection could be related to other diverse functions of POMC neurons, including secretion of  $\beta$ -endorphin, a neuropeptide that inhibits activity in gonadotropin-releasing hormone-expressing neurons in reproductive circuits<sup>24</sup> and also modulates reward circuits<sup>25</sup>. Nevertheless, this finding highlights the unbiased nature of LSPS as a search tool for presynaptic neuron location and that its use can identify projections in advance of an understanding of their function. Overall, these results establish that both fasting and leptin have dynamic effects on hypothalamic microcircuits.

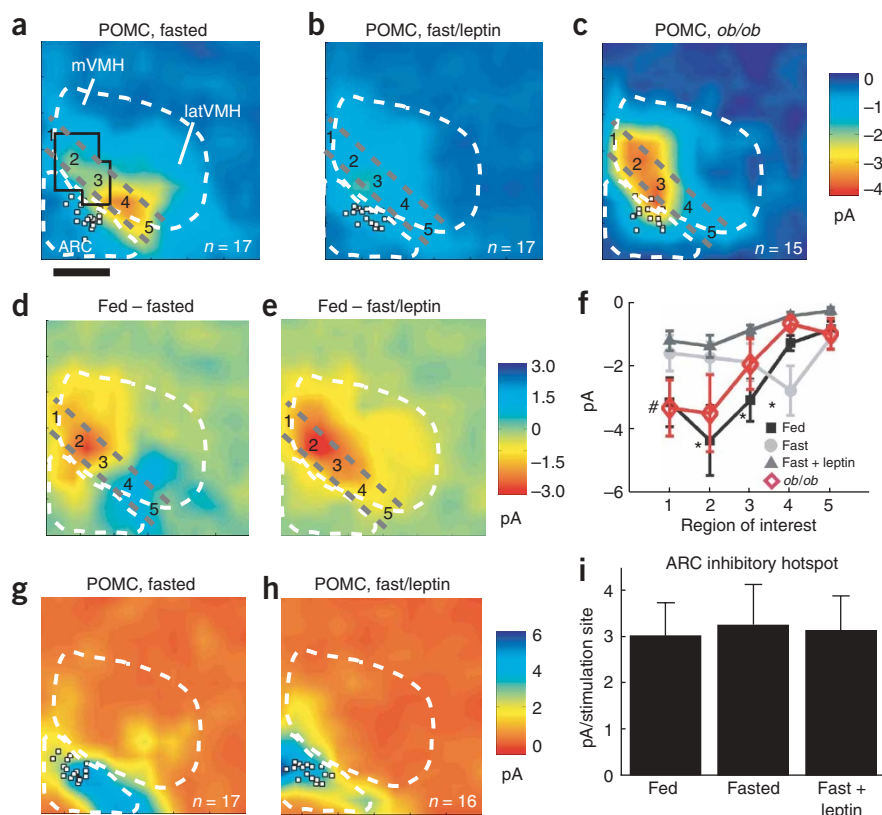


**Figure 5** Analysis of circuit plasticity after fasting and with leptin treatment during fasting. (**a–c**) Mean excitatory synaptic input maps for POMC neurons in (**a**) mice after a 24 h fast, (**b**) fasted mice that received leptin and (**c**) *ob/ob* mice. (**d,e**) Difference maps were made by subtracting (**d**) fed minus fasted or (**e**) fed minus fasted with leptin treatment to illustrate sites of circuit plasticity. Negative values signify decreased excitatory synaptic input onto POMC neurons relative to the level in fed animals, and positive values signify increased excitatory inputs. Numbers along the diagonal gray dashed lines in **a–e** mark regions of interest. (**f**) Average current strength from regions of interest in the maps from fed, fasted and fasted + leptin-treated groups. #:  $P = 0.07$ , \*:  $P < 0.05$ , ANOVA. (**g,h**) Mean inhibitory synaptic input maps for POMC neurons from mice after (**g**) 24 h fast and from (**h**) fasted mice that received leptin. (**i**) Mean inhibitory synaptic input from the ARC hotspot. White squares mark soma locations. Scale bar: 300  $\mu\text{m}$ . Error bars are s.e.m.

## DISCUSSION

Physical<sup>2</sup>, chemical<sup>26</sup> or genetic<sup>4</sup> disruptions of the VMH cause obesity, and electrical stimulation of this nucleus causes a reduction of food intake<sup>27</sup>. While these data establish an important role for this nucleus in controlling food intake and body weight, the mechanisms by which the VMH regulates energy balance are largely unknown. In this report, we set out to test whether pathways exist through which the VMH might regulate the activity of specific classes of ARC neurons that are known to regulate food intake and body weight. We used LSPS to show a functional interaction between the VMH and POMC neurons in the ARC and identified an entirely new projection,  $\text{mVMH}^{\text{exc}} \rightarrow \text{ARC}^{\text{POMC}}$ . This projection carries excitatory inputs from the mVMH to POMC neurons in the ARC. Furthermore, we showed that this interaction is rapidly and significantly modified by changes in nutritional state. Notably, the medial VMH subdivisions have been previously associated with regulation of energy balance and metabolism, with both leptin-<sup>28</sup> and glucose-responsive neurons<sup>29</sup> localized there. In aggregate, these data suggest a pathway by which the mVMH might regulate energy balance through excitatory synaptic input to POMC neurons that suppress feeding.

In principle, the VMH could also mediate satiety by directly inhibiting NPY neurons. However, we did not find any evidence supporting this alternate pathway, as there were only sparse inputs to NPY neurons from the VMH, and these were spatially distinct excitatory inputs from the latVMH, a subregion that is known to regulate sexual behavior<sup>30,31</sup>. As NPY has been shown to regulate fertility, one possible role of  $\text{latVMH}^{\text{exc}} \rightarrow \text{ARC}^{\text{NPY}}$  may be to control aspects of reproductive behavior and neuroendocrine function. Although these data do not rule out the existence of mVMH connections to NPY neurons, the frequency of such connections is presumably far less than for POMC neurons.

Functional mapping showed markedly different spatial distributions of VMH inputs onto NPY versus POMC neurons in the ARC. A comparison of the NPY and POMC input maps with those from unlabeled ARC neurons ( $\text{VMH}^{\text{exc}} \rightarrow \text{ARC}^{\text{unknown}}$ ) suggests that the  $\text{mVMH}^{\text{exc}} \rightarrow \text{ARC}^{\text{POMC}}$  and  $\text{latVMH}^{\text{exc}} \rightarrow \text{ARC}^{\text{NPY}}$  comprise only a subset of the total excitatory projections to the ARC, indicating that there are other VMH projections onto unidentified ARC cell types. Overall, these data add several new elements to the wiring diagram of the VMH and the ARC (**Supplementary Fig. 1**) and demonstrate that different ARC neurons with diverse functions are integrated into spatially distinct synaptic circuits. These results highlight the added information that can be generated by using LSPS in animals in which specific neuronal cell types can be identified.

## Functional considerations for synaptic input maps

These results also illustrate the marked plasticity of hypothalamic circuits<sup>10,32,33</sup> in response to changes in nutritional state. The dynamic regulation of  $\text{mVMH}^{\text{exc}} \rightarrow \text{ARC}^{\text{POMC}}$  by food restriction and weight loss is consistent with a proposed anorexigenic function for this projection, and suggests that the hyperphagia that develops after food deprivation may result, in part, from a reduction of excitatory inputs from the mVMH to POMC neurons. However, the relative contribution to energy homeostasis of  $\text{mVMH}^{\text{exc}} \rightarrow \text{ARC}^{\text{POMC}}$  and the other microcircuits reported here remains to be established. An important future challenge will be to correlate activity in these circuits with specific biological responses *in vivo*. This will require the development of new approaches to modulate neuronal activity in molecularly defined microcircuits embedded within complex, poorly characterized brain regions. The identification of molecular markers for these mVMH neurons, such as neuropeptides, would allow the cell-specific targeting of novel gene cassettes that alter neuronal function. Techniques that permit the activation or silencing<sup>34,35</sup> of specific projections are under development and could be thus be used to assess the contribution of this specific neural circuit to feeding behavior. Our results represent a necessary first step towards linking specific neural circuits and feeding behavior by demonstrating distinct microcircuits to POMC and NPY

neurons and correlating the strength of one such microcircuit (mVMH<sup>exc</sup> → ARC<sup>POMC</sup>) with metabolic state.

### Technical considerations for synaptic input maps

In these studies, we identified ‘hotspots’ of synaptic input that were anatomically distinct for POMC and NPY neurons. These hotspots correspond to the location of neurons that project the strongest and most frequently observed synaptic inputs for each cell type. The interpretation that the mVMH<sup>exc</sup> → ARC<sup>POMC</sup> hotspot corresponds to presynaptic neuron location in the mVMH as opposed to dendritic stimulation of neurons in the ARC is based on three lines of evidence: (i) excitation profiles of ARC neurons show that maximal activation of the ARC neurons occurs near the soma (Fig. 2c), whereas in synaptic input maps onto POMC neurons, the strongest region of the hotspot extends well into the mVMH and not substantially into the ARC; (ii) inspection of synaptic input maps for individual POMC neurons shows that sites of synaptic input are localized to the VMH and typically do not extend into the ARC and (iii) Golgi studies indicate that ARC neurons only rarely extend dendrites into the main body of the VMH<sup>13</sup>. Notably, the hotspots reported here for different neuron subtypes are spatially quite distinct, further demonstrating that the spatial resolution in these studies is sufficient to identify distinct hypothalamic microcircuits.

An additional consideration is that the connections observed in these studies were restricted to intact projections within the brain slice preparation. By recording input maps to unlabeled ARC neurons, we determined the extent to which intact circuit connections could be reliably obtained in this coronal slice plane (Fig. 4a,b, left). We observed robust connectivity from across the ventral surface of this slice plane at both medial and lateral positions. There is clearly a fall-off in connectivity from sites at the dorsal VMH boundary that is likely due to an increased probability of cut connections, and the resulting data should not be interpreted as an absence of inputs from these regions. For this reason, LSPS is best suited for analysis of specific microcircuits, as opposed to a global analysis of all of the afferent inputs to a brain region. The focus of this study was to test functional connectivity between the VMH and the ARC and to dissect the origins of inputs from the VMH onto molecularly defined neurons in the ARC. For this aim, functional mapping is strong evidence for connectivity, which, in the case of VMH → ARC, had not been fully tested based on anatomical methods. It can be expected that glutamate uncaging in other brain slice orientations will demonstrate additional patterns of synaptic input to the molecularly defined neurons in the ARC.

In summary, we have used LSPS to map functional connections within the hypothalamus and identified a new excitatory circuit between the mVMH and POMC neurons in the ARC (mVMH<sup>exc</sup> → ARC<sup>POMC</sup>). By applying LSPS to molecularly defined, GFP-labeled neurons, we have observed a more refined spatial distribution of projections than was evident when using unlabeled neurons. We have also demonstrated that POMC and NPY neurons, which are interspersed in the ARC but have opposing effects on feeding, receive presynaptic inputs from anatomically distinct regions. The observed excitatory projection of mVMH neurons to anorexigenic POMC neurons and its diminution by fasting provide the basis for the hypothesis that the VMH reduces food intake by activating POMC neurons, a possibility that remains to be tested *in vivo*. Conversely, the absence of inhibitory inputs to NPY neurons from the VMH suggests that it is less likely that the VMH might promote satiety by directly inhibiting the activity of NPY neurons. Finally, we show that the use of LSPS in animals with GFP-labeled neurons allows the generation of detailed wiring diagrams of feeding circuits (Supplementary Fig. 1).

The approach used here may also prove valuable for identifying new molecularly defined neural circuits controlling other behaviors.

### METHODS

**Slice preparation, electrophysiology, glutamate uncaging.** Experimental techniques were similar to those reported previously<sup>17</sup>, and only the differences are described here. Animal care and experimentation followed Rockefeller University’s Care and Use guidelines. Only male mice (P23–P33) were used in this study. Fasted mice were deprived of food for 24 h. For one group of fasted animals, leptin (1 µg/g), was administered intraperitoneally (i.p.) at the start of the fast and after 12 h. Brain slices were always prepared within 1 h before the end of the dark cycle. Typically, one coronal slice (300 µm thickness) per animal was cut using a vibratome in chilled cutting solution containing (in mM): 110 choline chloride, 25 NaHCO<sub>3</sub>, 11 glucose, 2.5 KCl, 1.25 NaH<sub>2</sub>PO<sub>4</sub>, 11.6 sodium ascorbate, 3.1 sodium pyruvate, 7 MgCl<sub>2</sub>, 0.5 CaCl<sub>2</sub>, aerated in 95% O<sub>2</sub>/5% CO<sub>2</sub>. Slices were transferred to artificial cerebrospinal fluid (ACSF) containing (in mM): 119 NaCl, 25 NaHCO<sub>3</sub>, 11 glucose, 2.5 KCl, 1.25 NaH<sub>2</sub>PO<sub>4</sub>, 4 MgCl<sub>2</sub>, 4 CaCl<sub>2</sub>, aerated in 95% O<sub>2</sub>/5% CO<sub>2</sub>. High divalents were used to reduce spontaneous synaptic activity. The slice was incubated at 34 °C for ~30 min and then transferred to a recording chamber containing ACSF with 0.24 mM caged, MNI-glutamate (4-methoxy-7-nitroindolyl 1-glutamate, Tocris) at 22 °C. Neurons were identified by fluorescence emission and then visually targeted with infrared gradient contrast optics. Neurons > 35 µm from the surface of the slice were patched using electrodes with tip resistances 3.5–5 MΩ. The intracellular solution contained (in mM): 132 cesium trifluoromethanesulfonate, 7 CsCl, 10 HEPES, 4 Mg<sub>2</sub>ATP, 0.3 Na<sub>2</sub>GTP, 10 sodium phosphocreatine, 3 sodium ascorbate, 1 EGTA, 0.05 Alexa-594 (Molecular Probes). Series resistances were 13–30 MΩ. Input resistances were > 1 GΩ. Excitatory postsynaptic currents were isolated at the holding potential –62 to –58 mV. Inhibitory postsynaptic currents were isolated at the reversal potential of the glutamate-activated current (0 to +12 mV). Laser stimulus was 1 ms.

**Data analysis.** Data analysis was similar to that reported previously<sup>17</sup>, and only the differences are described here. Responses were analyzed for 75 ms after the ultraviolet stimulus for excitatory PSCs and 250 ms for inhibitory PSCs owing to their larger amplitude and slower decay time. The first 5 ms was parsed into direct responses, and the remaining time was the synaptic window. Typically, two to four maps were obtained for each cell and were averaged, reducing noise due to spontaneous PSCs. Note that the contribution of spontaneous PSCs was small, and these magnitudes were not statistically different between sample populations. These averaged single maps were then averaged across all of the cells recorded into a group map for each cell type or experimental condition. This was done by aligning the uncaging pattern to the base of the brain and the third ventricle so that maps were recorded with the same orientation. Post-recording, slices were fixed, stained with 1% Sytox Green (Molecular Probes) in phosphate buffer/0.3% Triton-100, and fluorescence emission was used to visualize anatomical boundaries (Fig. 1i). Images were overlaid with brightfield images of the slice in the recording chamber using the third ventricle, base of the brain and other anatomical markings for alignment. In this way, anatomical boundaries of each slice could be mapped onto specific pixels in the synaptic input maps. In group maps, average anatomical boundaries were calculated for display purposes. Also, for display only, the averaged group maps were filtered with a two dimensional Gaussian (sigma: 49 µm, tiling: 3 × 3) to smooth the maps. Data collection and data analysis were performed using software written in Matlab (Mathworks).

*Note: Supplementary information is available on the Nature Neuroscience website.*

### ACKNOWLEDGMENTS

We are grateful to K. Svoboda for his generous assistance in implementing LSPS (funding to K.S. from the Howard Hughes Medical Institute (HHMI)) and to X.-L. Cai for assistance with mouse breeding. Support by Helen Hay Whitney Foundation (S.M.S.), HHMI (G.M.G.S., J.M.F.) and the US National Institutes of Health (J.M.F.).

### COMPETING INTERESTS STATEMENT

The authors declare that they have no competing financial interests.

Published online at <http://www.nature.com/natureneuroscience/>  
 Reprints and permissions information is available online at <http://npg.nature.com/reprintsandpermissions/>

1. Kennedy, G.C. The hypothalamic control of food intake in rats. *Proc. R. Soc. Lond. B* **137**, 535–549 (1950).
2. Hetherington, A.W. & Ranson, S.W. Hypothalamic lesions and adiposity in the rat. *Anat. Rec.* **78**, 149–161 (1940).
3. Anand, B.K. & Brobeck, J.R. Hypothalamic control of food intake in rats and cats. *Yale J. Biol. Med.* **24**, 123–140 (1951).
4. Majdic, G. *et al.* Knockout mice lacking steroidogenic factor 1 are a novel genetic model of hypothalamic obesity. *Endocrinology* **143**, 607–614 (2002).
5. Elmquist, J.K., Elias, C.F. & Saper, C.B. From lesions to leptin: hypothalamic control of food intake and body weight. *Neuron* **22**, 221–232 (1999).
6. Clark, J.T., Kalra, P.S., Crowley, W.R. & Kalra, S.P. Neuropeptide Y and human pancreatic polypeptide stimulate feeding behavior in rats. *Endocrinology* **115**, 427–429 (1984).
7. Zarjevski, N., Cusin, I., Vettor, R., Rohner-Jeanrenaud, F. & Jeanrenaud, B. Chronic intracerebroventricular neuropeptide-Y administration to normal rats mimics hormonal and metabolic changes of obesity. *Endocrinology* **133**, 1753–1758 (1993).
8. Huszar, D. *et al.* Targeted disruption of the melanocortin-4 receptor results in obesity in mice. *Cell* **88**, 131–141 (1997).
9. Fan, W., Boston, B.A., Kesterson, R.A., Hruby, V.J. & Cone, R.D. Role of melanocortinergic neurons in feeding and the agouti obesity syndrome. *Nature* **385**, 165–168 (1997).
10. Pinto, S. *et al.* Rapid rewiring of arcuate nucleus feeding circuits by leptin. *Science* **304**, 110–115 (2004).
11. DeFallo, J. *et al.* Virus-assisted mapping of neural inputs to a feeding center in the hypothalamus. *Science* **291**, 2608–2613 (2001).
12. Canteras, N.S., Simerly, R.B. & Swanson, L.W. Organization of projections from the ventromedial nucleus of the hypothalamus: a Phaseolus vulgaris-leucoagglutinin study in the rat. *J. Comp. Neurol.* **348**, 41–79 (1994).
13. van den Pol, A.N. & Cassidy, J.R. The hypothalamic arcuate nucleus of rat—a quantitative Golgi analysis. *J. Comp. Neurol.* **204**, 65–98 (1982).
14. Callaway, E.M. & Katz, L.C. Photostimulation using caged glutamate reveals functional circuitry in living brain slices. *Proc. Natl. Acad. Sci. USA* **90**, 7661–7665 (1993).
15. Sawatari, A. & Callaway, E.M. Convergence of magno- and parvocellular pathways in layer 4B of macaque primary visual cortex. *Nature* **380**, 442–446 (1996).
16. Dantzer, J.L. & Callaway, E.M. Laminar sources of synaptic input to cortical inhibitory interneurons and pyramidal neurons. *Nat. Neurosci.* **3**, 701–707 (2000).
17. Shepherd, G.M., Polgruto, T.A. & Svoboda, K. Circuit analysis of experience-dependent plasticity in the developing rat barrel cortex. *Neuron* **38**, 277–289 (2003).
18. Brivanlou, I.H., Dantzer, J.L., Stevens, C.F. & Callaway, E.M. Topographic specificity of functional connections from hippocampal CA3 to CA1. *Proc. Natl. Acad. Sci. USA* **101**, 2560–2565 (2004).
19. Yoshimura, Y., Dantzer, J.L. & Callaway, E.M. Excitatory cortical neurons form fine-scale functional networks. *Nature* **433**, 868–873 (2005).
20. Shepherd, G.M., Stepanyants, A., Bureau, I., Chklovskii, D. & Svoboda, K. Geometric and functional organization of cortical circuits. *Nat. Neurosci.* **8**, 782–790 (2005).
21. Callaway, E.M. Cell type specificity of local cortical connections. *J. Neurocytol.* **31**, 231–237 (2002).
22. Cowley, M.A. *et al.* Leptin activates anorexigenic POMC neurons through a neural network in the arcuate nucleus. *Nature* **411**, 480–484 (2001).
23. Ahima, R.S. *et al.* Role of leptin in the neuroendocrine response to fasting. *Nature* **382**, 250–252 (1996).
24. Faletti, A.G. *et al.* beta-Endorphin blocks luteinizing hormone-releasing hormone release by inhibiting the nitric oxide pathway controlling its release. *Proc. Natl. Acad. Sci. USA* **96**, 1722–1726 (1999).
25. Kreek, M.J. Methadone-related opioid agonist pharmacotherapy for heroin addiction. History, recent molecular and neurochemical research and future in mainstream medicine. *Ann. NY Acad. Sci.* **909**, 186–216 (2000).
26. Shimizu, N., Oomura, Y., Plata-Salaman, C.R. & Morimoto, M. Hyperphagia and obesity in rats with bilateral ibotenic acid-induced lesions of the ventromedial hypothalamic nucleus. *Brain Res.* **416**, 153–156 (1987).
27. Stenger, J., Fournier, T. & Bielajew, C. The effects of chronic ventromedial hypothalamic stimulation on weight gain in rats. *Physiol. Behav.* **50**, 1209–1213 (1991).
28. Elmquist, J.K., Bjorbaek, C., Ahima, R.S., Flier, J.S. & Saper, C.B. Distributions of leptin receptor mRNA isoforms in the rat brain. *J. Comp. Neurol.* **395**, 535–547 (1998).
29. Ono, T. *et al.* Glucocorticoid responsive neurons in rat ventromedial hypothalamic tissue slices *in vitro*. *Brain Res.* **232**, 494–499 (1982).
30. Christensen, L.W., Nance, D.M. & Gorski, R.A. Effects of hypothalamic and preoptic lesions on reproductive behavior in male rats. *Brain Res. Bull.* **2**, 137–141 (1977).
31. Pfaff, D.W. & Sakuma, Y. Deficit in the lordosis reflex of female rats caused by lesions in the ventromedial nucleus of the hypothalamus. *J. Physiol. (Lond.)* **288**, 203–210 (1979).
32. Theodosios, D.T. & Poulain, D.A. Activity-dependent neuronal-glia and synaptic plasticity in the adult mammalian hypothalamus. *Neuroscience* **57**, 501–535 (1993).
33. Bouret, S.G., Draper, S.J. & Simerly, R.B. Trophic action of leptin on hypothalamic neurons that regulate feeding. *Science* **304**, 108–110 (2004).
34. Slimko, E.M., McKinney, S., Anderson, D.J., Davidson, N. & Lester, H.A. Selective electrical silencing of mammalian neurons *in vitro* by the use of invertebrate ligand-gated chloride channels. *J. Neurosci.* **22**, 7373–7379 (2002).
35. Lechner, H.A., Lein, E.S. & Callaway, E.M. A genetic method for selective and quickly reversible silencing of mammalian neurons. *J. Neurosci.* **22**, 5287–5290 (2002).